Antenna Topology Optimization for Distributed Integrated Sensing and Communication

Kaitao Meng*, Kawon Han*, and Christos Masouros*
*Department of Electronic and Electrical Engineering, University College London, UK
Emails: *{kaitao.meng, kawon.han, c.masouros}@ucl.ac.uk

***Abstract*—We propose a cooperative integrated sensing and communication (ISAC) architecture that integrates coordinated multi-point (CoMP) communication with multi-static sensing. This study investigates how the allocation of a fixed total number of antennas among base stations (BSs) affects sensing and communication performance, and optimizes both the antenna topology and the number of BSs. To this end, we formulate an antenna topology optimization problem to balance the advantages of centralized and distributed antennas. Specifically, centralized antennas enhance beamforming and coherent processing in massive multiple-input and multiple-output (MIMO) systems, while distributed antennas improve spatial diversity and reduce access distances in cell-free setups. For sensing, we evaluate two localization methods, angle-of-arrival (AOA)-based and time-of-flight (TOF)-based localizations, to analyze how their scaling laws affect overall network performance. We analyze and demonstrate that the synchronization errors in our proposed architecture are negligible, thereby providing theoretical support for system implementation. In terms of communication, our results indicate that higher path loss exponents favour distributed configurations, while lower exponents benefit centralized setups. Simulations confirm that our cooperative scheme outperforms non-cooperative approaches, surpassing purely centralized or distributed strategies.**

I. Introduction

Given rising spectrum scarcity and interference issues between separate sensing and communication (S&C) systems, integrated sensing and communication (ISAC) has attracted significant academic and industrial interest [1]–[3]. ISAC leverages unified infrastructure and waveforms to simultaneously transmit information and receive echoes, thereby enhancing spectrum, cost, and energy efficiency [4]. Due to limited link-level ISAC coverage, attention has shifted towards network-level ISAC, where multiple base stations (BSs) cooperate through multi-cell S&C coordination [5], [6].

Network-level ISAC offers expanded coverage, improved service quality, flexible performance tradeoffs, and richer target information [7]–[9]. By exploiting both monostatic (BS-to-target-to-originating BS) and bistatic (BS-to-target-to-other BSs) links, cooperative BSs can maximize sensing capabilities. Moreover, coordinated multi-point (CoMP) techniques mitigate inter-cell interference and boost communication by linking a user to multiple BSs for enhanced reliability and throughput [10]. Although prior studies have examined network-level S&C tradeoffs through waveform design and cluster optimization [11], [12], few have addressed how antenna topology influences overall performance.

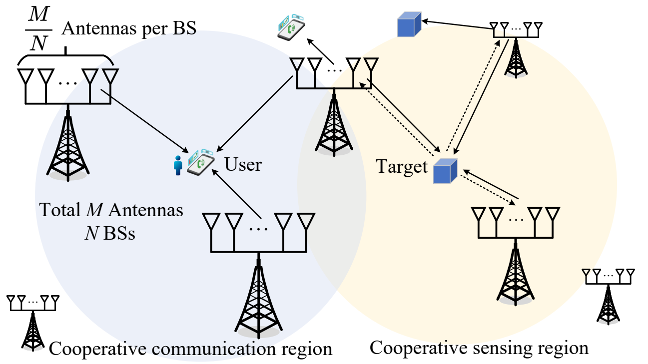

Fig. 1. Illustration of antenna-to-BS allocation in cooperative ISAC networks with optimized BS density.

Optimal antenna-to-BS allocation, defined by the number of antennas per site, is crucial for maximizing cooperative gains, as sensing and communication have different configuration requirements. Generally, allocation strategies are categorized as centralized or distributed. Centralized MIMO systems concentrate antennas at one site to simplify deployment and reduce costs, as in conventional cellular networks [13]. In contrast, distributed MIMO (e.g., cell-free systems) disperses antennas to mitigate channel correlation, enhance spatial diversity, and shorten access distances [14].

We propose a cooperative ISAC scheme that integrates centralized and distributed strategies to optimize the tradeoff between beamforming gain and geometric diversity. Specifically, concentrating antennas enhances beamforming gain, but it also extends the average service distance, which may compromise performance over larger areas. In contrast, distributing antennas improves sensing and communication quality over shorter distances. Although previous studies have optimized antenna configurations based on specific user or target locations [15], practical uncertainties in the positions of users, targets, and BSs, as well as channel fading, necessitate the development of new antenna topology analysis method.

As shown in Fig. 1, in the proposed scheme, multiple BSs within a communication region jointly transmit the same data, while another BS set in cooperative sensing region collaborates on target localization. By integrating CoMP-based joint transmission with multi-static sensing, our approach achieves a balance between sensing and communication at the network level. We evaluate two localization methods, angle-of-arrival (AOA)-based and time-of-flight (TOF)-

ISBN 978-3-903176-73-7

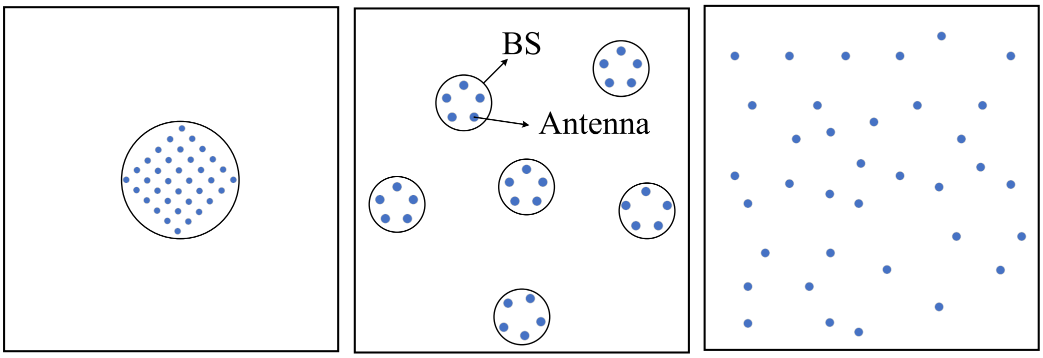

(a) Massive MIMO (b) Flexible deployment (c) Cell-free MIMO

Fig. 2. Illustration of different types of antenna topologies

based, to assess the impact of antenna-to-BS allocation on network performance, revealing the following scaling laws: the localization error of TOF-based methods scale as $1/\ln^2 N$, and AOA-based as $1/\ln N$, where N denotes the number of BSs involving into the localization process. For communication, the determination of optimal antenna-to-BS allocation shows that larger path loss exponents favour distributed configurations to reduce access distances, whereas smaller exponents favour centralized setups to maximize beamforming gain. A performance boundary optimization demonstrates that cooperative transmission and sensing can effectively improve S&C gains while offering a flexible tradeoff between the two functionalities.

II. System Model

A. Cooperation ISAC Framework

As shown in Fig. 1, BSs within a circle of radius D (centered at the target/user) form a cooperative cluster. For communication, these BSs use CoMP by transmitting identical signals to enhance received power via constructive superposition over power domain. For target localization, they operate as a distributed multi-static MIMO radar employing code-division multiplexing to ensure waveform orthogonality. Given the high cost and inherent complexity of achieving phase-level synchronization, our design strategically opts for non-coherent joint transmission paired with non-coherent MIMO radar processing. This approach not only simplifies system implementation but also maintains a balanced performance-to-feasibility ratio by minimizing synchronization overhead. In parallel, this study investigates the optimal allocation of antennas in cooperative ISAC networks while operating under a fixed total antenna resource constraint. On one hand, centralized antenna arrays are advantageous because they enhance beamforming precision and yield significant coherent gains, as shown in Fig 2(a), which are critical for precise target detection and efficient signal focusing. On the other hand, distributing antennas across different nodes increases macro-multiplexing capacity and offers improved spatial diversity, as shown in Fig 2(c), thereby enhancing robustness in communication links and radar detection in complex environments. By carefully analyzing these factors, our proposed scheme adeptly navigates the tradeoffs between achieving high coherent gain through centralized arrays, exploiting macro-multiplexing benefits, and leveraging geometric diversity, as illustrated in Fig 2(b). This balanced approach ensures that the system effectively meets both sensing and communication performance requirements, making it a robust solution for modern ISAC networks.

With a fixed total number of antennas of the given region, i.e., fixed antenna density, we optimize the antenna number per BS, as shown Fig. 1. Define antenna density as antennas per km^2 and BS density as BSs per km^2. Given transmit and receive antenna densities λ_t and λ_r, and assuming each BS employs a uniform linear array, the BS density is $\lambda_b = \frac{\lambda_t}{M_t} = \frac{\lambda_r}{M_r}$, where M_t and M_r represent the number of transmit and receive antennas per BS, respectively. Assuming a fixed overall antenna density, increasing the number of antennas per BS inevitably reduces the total BS density. We model the BS locations as a homogeneous Poisson point process (PPP) in a two-dimensional space, represented by $\Phi_b = \{\mathbf{d}_i = [x_i, y_i]^T \in \mathbb{R}^2 : i \in \mathbb{N}^+\}$, where each $\mathbf{d}_i$ specifies the position of BS i.

Each BS employs transmit precoding (TPC) to simultaneously deliver the information signal $s^c(t)$ to its served user and a dedicated radar signal $s_i^s(t)$ for target localization, where t denotes the time instant. We assume that $\mathrm{E}[s_i^s(t)(s_i^c)^H(t)] = 0$. For simplicity, the time argument (t) is omitted from the S&C signal notation in the following discussion. By defining $\mathbf{s}_i = [s_i^s, s_i^c]^T$, we obtain $\mathrm{E}\left[\mathbf{s}_i\mathbf{s}_i^H\right] = \mathbf{I}_2$. Then, the signal transmitted by the ith BS is given by

$$\mathbf{x}_i = \mathbf{W}_i\mathbf{s}_i = \mathbf{w}_i^c s_i^c + \mathbf{w}_i^s s_i^s, \tag{1}$$

where $\mathbf{w}_i^c$ and $\mathbf{w}_i^s \in \mathbb{C}^{M_t\times 1}$ are TPC vectors, with $\|\mathbf{w}_i^c\|^2 = p^c$ and $\|\mathbf{w}_i^s\|^2 = p^s$. Here, p^s and p^c denote the transmit power allocated to the sensing and communication signals, respectively, and $\mathbf{W}_i = [\mathbf{w}_i^c, \mathbf{w}_i^s] \in \mathbb{C}^{M_t\times 2}$ represents the TPC matrix for the BS located at $\mathbf{d}_i$. To eliminate interference between the S&C functions and simplify the analysis, we employ local zero-forcing (ZF) beamforming. Then, the beamforming matrix of the serving BS i is given by $\mathbf{W}_i = \tilde{\mathbf{W}}_i\left(\sqrt{\mathrm{diag}\left(\tilde{\mathbf{W}}_i^H\tilde{\mathbf{W}}_i\right)}\right)^{-1}$, where $\tilde{\mathbf{W}}_i = \mathbf{H}_i(\mathbf{H}_i^H\mathbf{H}_i)^{-1}$

and $\mathbf{H}_i = [(\mathbf{h}_{i,c}^H)^T, (\mathbf{a}^H(\theta_i))^T]^T$. Here, $\mathbf{h}_{i,c}^H \in C^{M_t \times 1}$ denotes the communication channel spanning from BS i to the typical user, and $\mathbf{a}^H(\theta_i) \in C^{M_t \times 1}$ represents the sensing channel impinging from BS i to the typical target. We have $p^s + p^c = 1$ with normalized transmit power.

B. Cooperative Sensing Model

We investigate the optimal antenna-to-BS allocation by analyzing the scaling behavior of target localization techniques based on AOA measurements, TOF measurements, and their combination. Assuming unbiased estimates, the CRLB provides a theoretical benchmark for localization accuracy measured in mean squared error (MSE). A typical target is collaboratively sensed by N BSs, and we assume that the radar signals $\{s_i^s\}_{i=1}^N$ transmitted by the BSs in the cooperative sensing cluster are approximately orthogonal for any time delay of interest [16]. The base-band equivalent signal impinging on receiver j is expressed as

$$\mathbf{y}_j(t)=\sum\nolimits_{i=1}^{N}\sigma d_j^{-\frac{\beta}{2}}\mathbf{b}\left(\theta_j\right) d_i^{-\frac{\beta}{2}}\mathbf{a}^H(\theta_i)\mathbf{W}_i\boldsymbol{s}_i(t-\tau_{i,j})+\mathbf{n}_l(t), \tag{2}$$

where $d_i = \|\mathbf{d}_i\|$ represents the distance from BS i to the origin, and $\beta \geq 2$ is the pathloss exponent between the serving BS and the typical target. Moreover, σ denotes the radar cross section (RCS), $\tau_{i,j}$ is the propagation delay for the link from BS i to the target and then to BS j. The term $\mathbf{n}_l(t)$ is the additive complex Gaussian noise with zero mean and covariance matrix $\sigma_s^2\mathbf{I}_{M_r}$. Additionally, the steering vector is given by $\mathbf{a}^H(\theta_i) = [1, \cdots, e^{j\pi(M_t-1)\cos(\theta_i)}]$, and the receiver response vector is $\mathbf{b}(\theta_j) = [1, \cdots, e^{j\pi(M_r-1)\cos(\theta_j)}]^T$, where θ_i denotes the bearing angle from BS i to the target with respect to the horizontal axis. The cooperative sensing model ignores interference from echoes of other targets since distinct spatial positions, angles, and propagation delays enable advanced filtering techniques, such as adaptive filtering.

1) AOA Measurement based Localization: For the AOA estimate at the receiver j, the covariance matrix can be given by $\mathbf{R}_y = \mathbb{E}\left\{\mathbf{y}_j(t)\mathbf{y}_j^H(t)\right\}$, and perform an eigen-decomposition to separate the signal and noise subspaces. The MUSIC algorithm can be applied to this decomposition to generate a pseudospectrum, where the peak corresponds to the estimated AOA [17]. By measuring the AOAs of each monostatic link and bi-static link, the target location can be estimated by maximum likelihood estimation [18]. The location of a typical target is denoted as $\boldsymbol{\psi}_t = [x_t, y_t]^T$. For the AOA measurement of the bi-static link from the jth BS to the target and then to the ith BS, we have

$$\hat{\theta}_{i,j} = \tan^{-1}\frac{y_t - y_i}{x_t - x_i} + n_{i,j}^a. \tag{3}$$

In (3), $n_{i,j}^a$ denotes the AOA measurement error, and $n_{i,j}^a \sim \mathcal{N}\left(0, \rho_{i,j}^2\right)$, where $\rho_{i,j}^2 = \frac{6}{\pi^2\cos^2\theta_i M_r(M_r^2-1)G_t\gamma_{i,j}}$ [19] and $\gamma_{i,j} = \frac{\sigma p^s\gamma_0}{d_i^\beta d_j^\beta}$. Here, G_t is the TPC gain, and γ_0 represents the channel power at the reference distance of 1 m. Then, we transform N^2 AOA measurement links into the target location. The Jacobian matrices of the N BS measurement errors, evaluated at the true target position $\boldsymbol{\psi}_t = [x_t, y_t]^T$, indicate

$$\mathbf{J}_{\mathrm{A}} = \begin{bmatrix} \frac{\partial\hat{\theta}_1}{\partial x_t} & \frac{\partial\hat{\theta}_1}{\partial y_t} \\ \vdots & \vdots \\ \frac{\partial\hat{\theta}_N}{\partial x_t} & \frac{\partial\hat{\theta}_N}{\partial y_t} \end{bmatrix} = \begin{bmatrix} \frac{-\sin\theta_1}{d_1} & \frac{\cos\theta_1}{d_1} \\ \vdots & \vdots \\ \frac{-\sin\theta_N}{d_N} & \frac{\cos\theta_N}{d_N} \end{bmatrix}_{N\times 2}. \tag{4}$$

Then, the Fisher information matrix (FIM) of estimating the target location for the AOA-based MIMO radar considered is equal to

$$\begin{aligned}\mathbf{F}_{\mathrm{A}} &= \tilde{\mathbf{J}}_{\mathrm{A}}^T\boldsymbol{\Sigma}_{\mathrm{A}}^{-1}\tilde{\mathbf{J}}_{\mathrm{A}} \\ &= |\zeta_a|^2\sum\nolimits_{j=1}^{N}\sum\nolimits_{i=1}^{N}\frac{\cos^2\theta_i}{d_j^2 d_i^2}\begin{bmatrix} \frac{\sin^2\theta_i}{d_i^2} & -\frac{\sin\theta_i\cos\theta_i}{d_i^2} \\ -\frac{\sin\theta_i\cos\theta_i}{d_i^2} & \frac{\cos^2\theta_i}{d_i^2}\end{bmatrix},\end{aligned} \tag{5}$$

where $\tilde{\mathbf{J}}_{\mathrm{A}} = \left[\mathbf{J}_{\mathrm{A}}^T, \cdots, \mathbf{J}_{\mathrm{A}}^T\right]^T \in \mathbb{C}^{N^2\times 2}$, $\boldsymbol{\Sigma}_{\mathrm{A}} = \mathrm{diag}(\rho_{1,1}^2, \cdots, \rho_{i,j}^2, \cdots, \rho_{N,N}^2) \in \mathbb{C}^{N^2\times N^2}$, and $|\zeta_a|^2 = \frac{1}{6}\pi^2 M_r\left(M_r^2 - 1\right)G_t\sigma p^s\gamma_0/\sigma_s^2$ [2]. Given the random location of ISAC BSs, the expected CRLB for any unbiased estimator of the target position is given by

$$\mathrm{CRLB}_{\mathrm{A}} = \mathrm{E}_{\Phi_b, G_t}\left[\mathrm{tr}\left(\mathbf{F}_{\mathrm{A}}^{-1}\right)\right]. \tag{6}$$

In (6), the expectation encompasses both the randomness of the BS locations and the variations in received beam power due to user channel fluctuations, thereby yielding the network's average sensing performance bound.

2) TOF Measurement based Localization: From transmitter j to the target and then to receiver i, the distance d_{ij} between the jth transmitter and the ith receiver is modeled as

$$\hat{d}_{ij}(\tau_{ij}) = d_{ij} + n_{ij}^r, \tag{7}$$

where $n_{ij}^r \sim \mathcal{N}\left(0, \eta_{ij}^2\right)$ and $\eta_{ij}^2 = \frac{3c^2\sigma_s^2}{2\pi^2 G_t M_r B^2\gamma_{ij}}$. Here, c represents the speed of light, and B^2 indicates the squared effective bandwidth, implying that a larger bandwidth results in a more precise TOF estimation. To estimate the range $\hat{d}_{ij}$ based on TOF, we apply matched filtering to the received signal by correlating it with a replica of the transmitted waveform. This procedure accentuates peaks associated with target-induced time delays, which are subsequently converted into range estimates using the speed of light. For signals emanating from transmitter i, the Jacobian matrices corresponding to the measurement errors at the N receivers, evaluated at the target position, are given by

$$\mathbf{J}_{\mathrm{R}}^T = \begin{bmatrix} \frac{\partial d_{11}}{\partial x_t} & \ldots & \frac{\partial d_{ij}}{\partial x_t} & \ldots & \frac{\partial d_{NN}}{\partial x_t} \\ \frac{\partial d_{11}}{\partial y_t} & \ldots & \frac{\partial d_{ij}}{\partial y_t} & \ldots & \frac{\partial d_{NN}}{\partial y_t}\end{bmatrix}, \tag{8}$$

where $\frac{\partial d_{ij}}{\partial x_t} = \cos\theta_i + \cos\theta_j$ and $\frac{\partial d_{ij}}{\partial y_t} = \sin\theta_i + \sin\theta_j$. Let $a_{ij} = \cos\theta_i + \cos\theta_j$ and $b_{ij} = \sin\theta_i + \sin\theta_j$. Then, the FIM of estimating the parameter vector $\boldsymbol{\psi}_t$ for the TOF measurement radar considered is equal to [20]

$$\begin{aligned}\mathbf{F}_{\mathrm{R}} &= \mathbf{J}_{\mathrm{R}}^T\boldsymbol{\Sigma}_{\mathrm{R}}^{-1}\mathbf{J}_{\mathrm{R}} \\ &= |\zeta_r|^2\sum\nolimits_{i=1}^{N}\sum\nolimits_{j=1}^{N} d_i^{-\beta}d_j^{-\beta}\begin{bmatrix} a_{ij}^2 & a_{ij}b_{ij} \\ a_{ij}b_{ij} & b_{ij}^2\end{bmatrix},\end{aligned} \tag{9}$$

where $\mathbf{\Sigma}_{\mathrm{R}} = \mathrm{diag}(\eta_{1,1}^2, \cdots, \eta_{i,j}^2, \cdots, \eta_{N,N}^2)$. In (9), we have [20]

$$|\zeta_r|^2 = \frac{8\pi^2 p^s G_t M_r B^2 \sigma \gamma_0}{c^2 \sigma_s^2}. \tag{10}$$

In (10), $|\zeta_r|$ is the common system gain term. Given the random location of ISAC BSs, the expected CRLB for any unbiased estimator of the target position is given by

$$\mathrm{CRLB}_{\mathrm{R}} = \mathrm{E}_{\Phi_b, G_t}\left[\mathrm{tr}\left(\mathbf{F}_{\mathrm{R}}^{-1}\right)\right]. \tag{11}$$

Similarly, the expectation encompasses both the randomness of the BS locations and the variations in received beam power.

3) Synchronization Error in TOF Measurement: To ensure optimal cooperative S&C performance in ISAC networks, precise time synchronization among BSs is essential. Specifically, timing misalignment introduces target localization errors in cooperative sensing, even under non-coherent cooperation. This is because the time offset between BSs leads to errors in TOF measurements over bistatic sensing links, thereby degrading localization accuracy. Considering synchronization errors, the TOF measurement model can be reformulated as [21]

$$\hat{d}_{ij}(\tau_{ij}) = d_{ij} + \tilde{d}_{ij}(\Delta t_{ij}) + n_{ij}^r, \tag{12}$$

where $\tilde{d}_{ij}(\Delta t_{ij})$ represents the distance error caused by the time offset Δt_{ij} between the jth transmitter and the ith receiver. It is important to note that there is no time offset for collocated transceivers, i.e., when $i = j$, implying $\Delta t_{ii} = 0, \forall i$. Since the distance error due to the time offset is an unknown random parameter, we employ the hybrid CRLB (HCRLB) to characterize the target localization accuracy as

$$\mathbf{F}_{\mathrm{H}} = \begin{bmatrix} \mathbf{J}_{\mathrm{R}}^T \mathbf{\Sigma}_{\mathrm{R}}^{-1} \mathbf{J}_{\mathrm{R}} & \mathbf{J}_{\mathrm{R}}^T \tilde{\mathbf{\Sigma}}_{\mathrm{R}}^{-1} \\ \tilde{\mathbf{\Sigma}}_{\mathrm{R}}^{-1} \mathbf{J}_{\mathrm{R}} & \tilde{\mathbf{\Sigma}}_{\mathrm{R}}^{-1} + \mathbf{\Sigma}_{\mathrm{P}}^{-1} \end{bmatrix}, \tag{13}$$

where $\tilde{\mathbf{\Sigma}}_{\mathrm{R}} = \mathrm{diag}(\eta_{1,2}^2, \cdots, \eta_{i,j}^2, \cdots, \eta_{N,N-1}^2) \in \mathbb{R}^{(N^2-N)\times(N^2-N)}$ excludes terms with $\eta_{i,i}^2, \forall i$, and $\mathbf{\Sigma}_{\mathrm{P}} = \mathrm{diag}(\delta_{1,2}^2, \cdots, \delta_{i,j}^2, \cdots, \delta_{N,N-1}^2) \in \mathbb{R}^{(N^2-N)\times(N^2-N)}$ denotes the variance of distance errors induced by time offsets in each bistatic link.

There are two main approaches to performing localization across N BSs, including centralized processing and decentralized processing. In centralized processing, all BSs send their received signal to a central node for joint parameter estimation, which typically achieves higher accuracy but requires more communication and computational overhead. In decentralized processing, each BS locally processes only its own received signals, and the BSs then exchange and fuse their local estimates, reducing communication overhead while potentially sacrificing some accuracy. Notably, the impact of time synchronization varies depending on the target localization scheme, specifically between decentralized and centralized processing [6]. While decentralized processing, where the target is localized independently at each local node, offers reduced data-sharing overhead, its accuracy is significantly affected by synchronization errors [21]. In contrast, centralized processing exhibits robustness to such errors, as monostatic measurements can compensate for synchronization-induced inaccuracies in bistatic measurements, thereby enabling more accurate target localization. In this work, we adopt centralized processing for target localization, whose performance can be approximately evaluated by (11) irrespective of synchronization errors. The above conclusion is verified in our simulations, as shown in Fig. 6. Importantly, this investigation also facilitates the extension of our analysis to antenna-to-BS allocation strategies under synchronization constraints and decentralized processing scenarios.

C. Cooperative Communication Model

Transmitters employ non-coherent joint transmission, meaning that the useful signals are combined through power accumulation. In our work, we adopt a user-centric clustering method where the BS closest to the typical user invites neighbouring BSs within a distance D to participate in cooperation. Consequently, the signal received at the typical user is expressed as

$$y_c = \underbrace{\sum\nolimits_{i\in\Phi_c} d_i^{-\frac{\alpha}{2}} \mathbf{h}_i^H \mathbf{W}_i \mathbf{s}_1}_{\text{collaborative intended signal}} + \underbrace{\sum\nolimits_{j\in\{\Phi_b\setminus\Phi_c\}} d_j^{-\frac{\alpha}{2}} \mathbf{h}_j^H \mathbf{W}_j \mathbf{s}_j}_{\text{inter-cluster interference}} + n_c, \tag{14}$$

where $\alpha \geq 2$ is the pathloss exponent, $\mathbf{h}_i^H \sim \mathcal{CN}\left(0, \mathbf{I}_{M_{\mathrm{t}}}\right)$ is the channel vector of the link between the BS at $\mathbf{d}_i$ to the typical user, Φ_c is the cooperative BS set, and n_c denotes the noise. In our analysis, the noise impact is neglected because interference from outside the cooperation region overwhelmingly dominates. The evaluation is based on the signal-to-interference ratio (SIR) [22]. The SIR of the received signal at the typical user can be expressed as

$$\mathrm{SIR}_c = \frac{\sum\limits_{i\in\Phi_c} g_i d_i^{-\alpha}}{\sum\limits_{j\in\{\Phi_b\setminus\Phi_c\}} g_j d_j^{-\alpha}}, \tag{15}$$

where $g_i = p^c \left|\mathbf{h}_i^H \mathbf{w}_i^c\right|^2$ denotes the channel gain of effective signals, and $g_j = p^c \left|\mathbf{h}_j^H \mathbf{w}_j^c\right|^2 + p^s \left|\mathbf{h}_j^H \mathbf{w}_j^s\right|^2$ represents the interference channel gain of BS j. The average data rate of users is given by

$$R_c = \mathrm{E}_{\Phi_b, g_i}[\log(1 + \mathrm{SIR}_c)]. \tag{16}$$

III. Sensing Performance Analysis

To simplify our analysis, we assume that the number of BSs within a distance D from each target is equal to the expected count given the PPP density.

A. Angle Measurement Based Localization

In this subsection, we derive the closed-form CRLB expression under the assumption of random locations of both the BSs and targets. We transform $\mathrm{CRLB_A}$ into

$$
\begin{aligned}
&\mathrm{E}_{\theta,d}\left[\frac{\sum_{i=1}^{N}\frac{f_i^2}{d_i^4}}{\sum_{j=1}^{N}\frac{1}{d_j^2}\left(\sum_{i=1}^{N}\frac{e_i^2}{d_i^4}\sum_{i=1}^{N}\frac{f_i^2}{d_i^4}-\left(\sum_{i=1}^{N}\frac{1}{d_i^4}e_if_i\right)^2\right)}\right]\\
=&\mathrm{E}_{\theta,d}\left[\frac{\sum_{i=1}^{N}\frac{f_i^2}{d_i^4}}{\sum_{j=1}^{N}\frac{1}{d_j^2}\left(\sum_{i=1}^{N}\sum_{i>j}^{N}\frac{1}{d_i^4d_j^4}(X_{i,j})^2\right)}\right],
\end{aligned}
\tag{17}
$$

where $X_{i,j}=\sin\theta_i\cos\theta_i\cos^2\theta_j-\sin\theta_j\cos\theta_j\cos^2\theta_i$, $e_i=\sin\theta_i\cos\theta_i$, and $f_i=\cos^2\theta_i$. When the number of nodes is large, the correlation between the numerator and the denominator becomes negligible, as the distances of different nodes are statistically independent under a PPP distribution. Moreover, when the number of nodes is large, the variability of the denominator is relatively small compared to its expected value. Then, CRLB can be approximated as

$$
\mathrm{CRLB_A}\approx\frac{16\sum_{i=1}^{N}\mathrm{E}[d_i]^{-\beta-2}}{3\sum_{k=1}^{N}\mathrm{E}[d_k]^{-\beta}\sum_{i=1}^{N}\sum_{i>j}^{N}\mathrm{E}[d_i]^{-\beta-2}\mathrm{E}[d_j]^{-\beta-2}}.
\tag{18}
$$

Furthermore, the expected distance from the nth closest BS to the typical target can be given by $E\left[d_n\right]=\frac{\Gamma\left(n+\frac{1}{2}\right)}{\sqrt{\lambda_b\pi}\Gamma(n)}\approx\sqrt{\frac{n}{\lambda_b\pi}}$. When $\beta=2$, we have $\lim\limits_{N\to\infty}\sum_{n=1}^{N}\frac{1}{n}\approx\ln N+\gamma+\frac{1}{2N}$ and $\lim\limits_{N\to\infty}\sum_{n=1}^{N}\frac{1}{n^2}\approx\frac{\pi^2}{6}$, where $\gamma=0.577$.

$$
\begin{aligned}
\mathrm{CRLB_A}\approx&\frac{\sum_{i=1}^{N}i^{-2}}{\frac{3}{32}\lambda_b^3\pi^3\left(\sum_{j=1}^{N}i^{-1}\right)\left(\left(\sum_{i=1}^{N}i^{-2}\right)^2-\sum_{i=1}^{N}i^{-4}\right)}\\
\approx&\frac{320}{3\lambda_b^3\pi^5\left(\ln N+\gamma+\frac{1}{2N}\right)}.
\end{aligned}
\tag{19}
$$

For optimal sensing performance, the transmit beamforming gain can be approximated as $\left\lfloor\frac{\lambda_tD^2\pi}{N}\right\rfloor$, and the BS density can be denoted by $\frac{N}{\pi D^2}$. Then, we have

$$
\begin{aligned}
\mathrm{CRLB_A}\approx&\frac{1}{|\tilde{\zeta}_a|^2\underbrace{\left\lfloor\frac{\lambda_rD^2\pi}{N}\right\rfloor^3}_{\text{Receive gain}}\underbrace{\left\lfloor\frac{\lambda_tD^2\pi}{N}\right\rfloor}_{\text{Transmit gain}}\underbrace{\frac{N^3}{(D^2\pi)^3}\pi^5\ln N}_{\text{Geometry gain}}}\\
\approx&\frac{320N}{3|\tilde{\zeta}_a|^2D^2\pi^6\lambda_t\lambda_r\ln N},
\end{aligned}
\tag{20}
$$

where $|\tilde{\zeta}_a|^2=\frac{1}{6}\pi^2\sigma p^s\gamma_0/\sigma_s^2$. According to (20), as the number of BSs increases, the value of $\mathrm{CRLB_A}$ also increases monotonically with N. Therefore, under fixed total transmit power constraints, a fully distributed antenna allocation is unlikely to be optimal. This is primarily because accurate AOA measurement relies on multiple antennas to enhance estimation accuracy.

Additionally, we examine a practical scenario in which the total transmit power across the region is fixed, implying that the BS transmit power scales linearly with the number of antennas. Consequently, the beamforming gain increases quadratically with the number of antennas, and then the corresponding CRLB is

$$
\mathrm{CRLB_A^{M_t}}\approx\frac{320N^2}{3|\tilde{\zeta}_a|^2D^4\pi^7\lambda_t^2\lambda_r\ln N}.
\tag{21}
$$

It is clear that, whether the system operates under a fixed total transmit power or scales power based on the number of antennas, when $N\gg1$, increasing the number of antenna locations (or BS density) while keeping the antenna density constant leads to a higher CRLB for the AOA-based localization method.

B. Range Measurement Based Localization

According to the derived scaling law in [11], for the fixed total transmit power constraints, we have

$$
\mathrm{CRLB_R}\approx\frac{2}{|\tilde{\zeta}_r|^2D^2\pi^2\lambda_t\lambda_r\ln^2N},
\tag{22}
$$

where $|\tilde{\zeta}_r|^2=\frac{8\pi^2p^sB^2\sigma\gamma_0}{c^2\sigma_s^2}$, According to (22), when the number of BSs is sufficiently large, the $\mathrm{CRLB_R}$ value decreases monotonically as the number of BSs N increases. Therefore, given the total BS power constraint, the TOF-based localization method tends to favor a distributed antenna allocation to achieve better sensing results at closer distances. Similarly, if the total power of each BS increases with M_t, we have

$$
\mathrm{CRLB_R^{M_t}}\approx\frac{2N}{|\tilde{\zeta}_r|^2D^4\pi^3\lambda_t^2\lambda_r\ln^2N}.
\tag{23}
$$

Based on (23), when the BS transmit power scales with the number of antennas, the optimal deployment will not be fully distributed because CRLB will grow as N approaches infinity.

IV. Communication Performance

To analyze the optimal antenna-to-BS allocation, we adopt simplifications for maximizing the expected SIR. First, we simplify the expected data rate as

$$
\mathrm{E}_{r,\Phi_b^S,g_i}\left[\ln\left(1+\frac{S}{I}\right)\right]\approx\mathrm{E}_r\left[\ln\left(1+\frac{\bar{S}_r}{\bar{I}_r}\right)\right],
\tag{24}
$$

where $\bar{S}_r=\mathrm{E}_{\Phi_b,g_i}[g_1+\sum_{i\in\Phi_a}g_i\left\|\mathbf{d}_i\right\|^{-\alpha}r^{\alpha}]=p^cr^{-\alpha}+\frac{\pi\lambda_b}{\alpha-2}\left(r^{-\alpha+2}-D^{-\alpha+2}\right)$ and $\bar{I}_r=\mathrm{E}_{\Phi_b,g_i}\left[\sum_{j\in\{\Phi_b\setminus\Phi_a\}}g_j\left\|\mathbf{d}_j\right\|^{-\alpha}r^{\alpha}\right]=\frac{\pi\lambda_b}{\alpha-2}D^{2-\alpha}$. Based on (24), we simplify the antenna allocation optimization by reformulating the objective from maximizing the expected spectral efficiency to maximizing the expected SIR, thereby streamlining the analysis. Then, it follows that

$$
\mathrm{E}_{r,\Phi_b^S,g_i}\left[\ln\left(1+\frac{S}{I}\right)\right]\approx\mathrm{E}_r\left[\ln\left(1+\overline{\mathrm{SIR}}\right)\right],
\tag{25}
$$

where $\overline{\mathrm{SIR}}=M_\mathrm{t}\left(\left(\frac{\alpha-2}{\pi\lambda_b}r^{-\alpha}+r^{-\alpha+2}\right)D^{\alpha-2}-1\right)$. In (25), we consider the optimal communication design, where the beamforming gain is M_t rather than $p^c(M_\mathrm{t}-1)$. The $\overline{\mathrm{SIR}}$ value increases monotonically with the size of cooperative regions D. Due to the complicated integral operation of the distance distribution r in (25), it is challenging to directly obtain the optimal antenna-to-BS allocation strategy based on (25). Thus, we analyze the relationship between the optimal number of antennas M_t and the expected SIR of the typical communication user. In the following, we use an approximate method for analysis, where a sufficiently small value of ϵ is chosen as the lower limit of integration to ensure the feasibility of the integral and the validity of the analysis.

$$\mathrm{E}_r\left[\frac{\bar{S}_r}{\bar{I}_r}\right] = \int_\epsilon^D M_{\mathrm{t}}\left(\frac{\frac{\alpha-2}{\pi\lambda_b}r^{-\alpha}+r^{-\alpha+2}}{D^{-\alpha+2}}-1\right)f_r(r)dr$$
$$= M_{\mathrm{t}}\Bigg(\frac{\alpha-2}{D^{-\alpha+2}}(\pi\lambda_b)^{\frac{\alpha-2}{2}}\int_\epsilon^{\pi\lambda_b D^2}u^{-\frac{\alpha}{2}}e^{-u}du$$
$$+\frac{(\pi\lambda_b)^{\frac{\alpha-2}{2}}}{D^{-\alpha+2}}\int_\epsilon^{\pi\lambda_b D^2}u^{\frac{-\alpha+2}{2}}e^{-u}du+e^{-\pi\lambda_b D^2}-1\Bigg)\triangleq G(M_{\mathrm{t}}). \tag{26}$$

Building on the above analysis, in the following, we investigate the optimal antenna-to-BS allocation in two specific cases.

Proposition 1: When $\alpha \to 2$, the optimal antenna-to-BS allocation strategy for communication is centralized, i.e., $\lambda_b^* = \frac{1}{\pi D^2}$ and $M_{\mathrm{t}}^* = \lambda_t \pi D^2$.

Proof: Let $\int_\epsilon^{\pi\lambda D^2} u^{-\frac{\alpha}{2}}e^{-u}du = \vartheta$. Upon substituting it into (26), due to $\lim\limits_{\epsilon\to 0}\int_\epsilon^{\pi\lambda_b D^2}u^{\frac{-\alpha+2}{2}}e^{-u}du = \gamma\left(1,\pi\lambda_b D^2\right)$, it follows that

$$\mathrm{E}\left[\frac{\bar{S}_r}{\bar{I}_r}\right] = M_{\mathrm{t}}\left(\vartheta+\gamma\left(1,\pi\lambda_b D^2\right)+e^{-\pi\lambda_b D^2}-1\right). \tag{27}$$

Due to $\gamma(1,x) = 1-e^{-x}$, $\mathrm{E}\left[\frac{\bar{S}_r}{\bar{I}_r}\right] = M_{\mathrm{t}}\vartheta$, we have $\vartheta > 0$ since $\mathrm{E}\left[\frac{\bar{S}_r}{\bar{I}_r}\right] \geq 0$. Therefore, the derivative of $G(M_{\mathrm{t}})$ follows

$$G'(M_{\mathrm{t}}) = \frac{\vartheta}{2} \geq 0. \tag{28}$$

Thus, given a region $|\mathcal{A}|$, the number of antennas is $|\mathcal{A}|\times\lambda_t$, and the expected SIR of the communication user increases upon increasing the number of antennas allocated at each location. Therefore, the optimal antenna-to-BS allocation strategy is centralized, i.e., $\lambda_b^* = \frac{1}{\pi D^2}$ and $M_{\mathrm{t}}^* = \lambda_t\pi D^2$. ■

Proposition 2: When $\alpha \gg 4$, the optimal antenna-to-BS allocation strategy for communication is distributed, i.e., $\lambda_b^* = \lambda_t$, $M_{\mathrm{t}}^* = 1$.

Proof: In (26), we have $\int_\epsilon^{\pi\lambda D^2}u^{-\frac{\alpha}{2}}e^{-u}du \approx \frac{2\epsilon^{-\frac{\alpha}{2}+1}}{\alpha-2}$ and $\int_\epsilon^{\pi\lambda D^2}u^{\frac{-\alpha+2}{2}}e^{-u}du \approx \frac{2\epsilon^{\frac{-\alpha+4}{2}}}{\alpha-4}$. Then, it follows that

$$G(M_{\mathrm{t}}) = M_{\mathrm{t}}\left(C_0 M_{\mathrm{t}}^{\frac{2-\alpha}{2}}+e^{-\frac{\pi\lambda_t D^2}{M_{\mathrm{t}}}}-1\right), \tag{29}$$

where $C_0 = \frac{2}{D^{-\alpha+2}}(\pi\lambda_t)^{\frac{\alpha-2}{2}}\epsilon^{-\frac{\alpha}{2}+1}\left(1+\frac{\epsilon}{\alpha-4}\right)$. Due to $\int_\epsilon^{\frac{\pi\lambda_t D^2}{M_{\mathrm{t}}}}u^{-\frac{\alpha}{2}}e^{-u}du \geq \frac{2\epsilon^{-\frac{\alpha}{2}+1}}{\alpha-2}$, the derivative of $G(M_{\mathrm{t}})$ becomes as follows

$$G'(M_{\mathrm{t}}) = \left(2\left(\frac{\pi\lambda_t D^2}{M_{\mathrm{t}}}\right)^{\frac{\alpha-4}{2}}\epsilon^{-\frac{\alpha}{2}+1}\left(1+\frac{\epsilon}{\alpha-4}\right)\frac{4-\alpha}{2}+1\right)$$
$$\times\frac{\pi\lambda_t D^2}{M_{\mathrm{t}}} \leq 0. \tag{30}$$

The inequality in (30) holds due to $2\left(\frac{\pi\lambda_t D^2}{M_{\mathrm{t}}}\right)^{\frac{\alpha-4}{2}}\epsilon^{-\frac{\alpha}{2}+1}\left(1+\frac{\epsilon}{\alpha-4}\right)\frac{4-\alpha}{2} \ll -1$ when $\alpha \gg 4$. Therefore, $G(M_{\mathrm{t}})$ increases, as M_{t} decreases. ■

The above conclusions provide practical guidance for antenna-to-BS allocation. In environments suffering from strong fading, a distributed antenna allocation strategy should be adopted for positioning service antennas closer to the users. In such scenarios, the distributed antenna allocation enhances the useful signal, because although the interference may be increased, the resulting mitigation of fading is typically more substantial. Conversely, in environments having mild fading, such as line-of-sight-dominant channels, distributed allocation may significantly amplify the interference and this is not outweighed by the fading mitigation. In these cases, a centralized allocation can be more effective, as beamforming techniques can be used to strengthen the desired signal, while reducing interference.

V. Sensing and Communication Tradeoffs

In this section, we analyze the optimization of cooperative ISAC networks to demonstrate that antenna-to-BS allocation introduces a new degree of freedom, enabling a flexible balance between sensing and communication performance. Based on the derivations in Sections III and IV, the derived tractable performance expressions of both S&C are functions of the number of antennas and BS density. Then, we present a performance metric, namely the rate-CRLB performance region, to verify the effectiveness of the proposed cooperative ISAC schemes. Without loss of generality, the S-C network performance region is defined as

$$\mathcal{C}_{c-s}(L,N,p^c,p^s) = \Big\{(\hat{r}_c,\hat{\mathrm{crlb}}) : \hat{r}_c \leq R_c, \hat{\mathrm{crlb}} \geq \mathrm{CRLB},$$
$$p^s+p^c \leq 1, M_{\mathrm{t}}\lambda_b \leq \lambda_t, M_{\mathrm{r}}\lambda_b \leq \lambda_r\Big\}, \tag{31}$$

where $(\hat{r}_c,\hat{\mathrm{crlb}})$ represents an achievable rate-CRLB performance pair. By investigating this region, we clearly see how enhancements in one aspect, such as increasing the communication rate, can influence another aspect, like localization accuracy, and vice versa. In essence, the rate-CRLB performance region acts as a framework that encapsulates every possible pair of communication rate and CRLB that can be achieved given a fixed allocation of antenna resources. A straightforward method to determine the boundary of this region is to perform an exhaustive search over all feasible variables $(M_{\mathrm{t}},\lambda_t,p^c,p^s)$ and then compute the corresponding sensing and communication performance metrics as outlined in Sections III and IV. However, this approach quickly becomes computationally burdensome, particularly when a large number of antennas are available.

Further analysis shows that the communication rate R_c increases monotonically with the communication transmit power p^c, while the CRLB decreases monotonically as the sensing transmit power p^s increases. Therefore, for a given power allocation, if the performance pair $(\hat{r}_c^*,\hat{\mathrm{crlb}}^*)$ at a specific base station (BS) density outperforms all other configurations $(\hat{r}_c',\hat{\mathrm{crlb}}')$, then the power distributions at these alternative BS densities cannot lie on the performance boundary. This insight allows us to simplify the search process by decoupling the two dimensions: rather than performing a two-dimensional exhaustive search over both BS density and p^c, we can examine each parameter

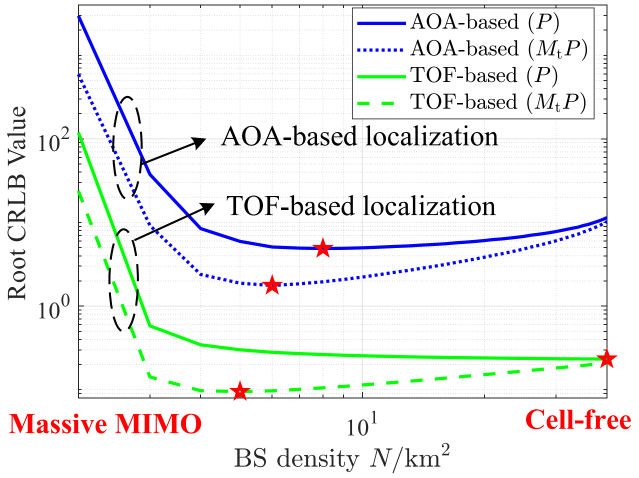

Fig. 3. Localization performance comparisons with respect to the cooperative BS density under the fixed antenna density (P and $M_t \cdot P$ refer to the total power constraint on each BS).

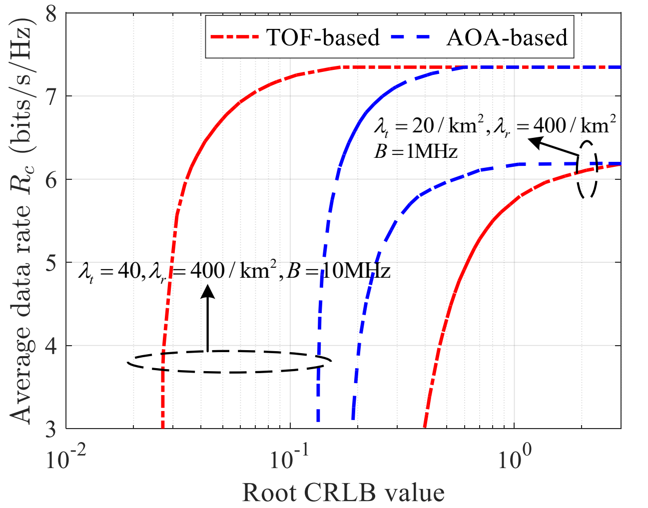

Fig. 5. Rate-CRLB performance boundary with different localization methods.

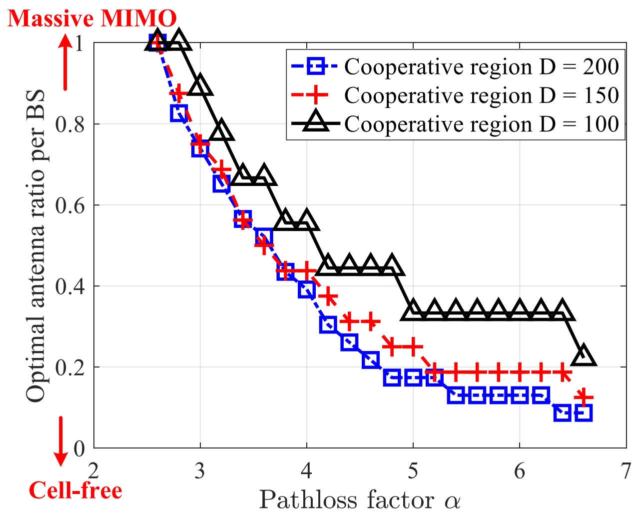

Fig. 4. Antenna allocation versus path loss factor α with various radius D = 100, 150, 200 m.

individually. Moreover, by identifying the optimal BS densities for communication-only and sensing-only networks, denoted by $\lambda_b^*(c)$ and $\lambda_b^*(s)$, respectively, the effective search interval can be narrowed significantly to the range $[\min(\lambda_b^*(c), \lambda_b^*(s)), \max(\lambda_b^*(c), \lambda_b^*(s))]$. This reduction not only lowers computational complexity but also sharpens our understanding of the trade-offs between communication and sensing performance.

VI. Simulations

Based on extensive numerical experiments, we investigated the core characteristics of ISAC networks and confirmed that our tractable expressions closely match the outcomes of Monte Carlo simulations. In our study, simulation results were averaged over various network configurations and small-scale fading scenarios. The system parameters include: $M_\mathrm{t} = 4$ transmit antennas, $M_\mathrm{r} = 10$ receive antennas, a per-BS transmit power of $P_\mathrm{t} = 1$ W, antenna densities $\lambda_t = \lambda_r = 50/\mathrm{km}^2$, an operating frequency of $f^c = 5$ GHz, a bandwidth $B \in [10, 100]$ MHz, a noise power of -100 dB, and pathloss exponents $\alpha = 4$ and $\beta = 2$.

In Fig. 3, both transmit and receive antenna densities are set to $50/\mathrm{km}^2$ with a noise level of $\sigma_s^2 = -100$ dB and a bandwidth of 10 MHz. In this figure, the legend distinguishes between a fixed energy allocation, denoted by P, which keeps each BS's total power constant regardless of the number of antennas, and a scenario where power scales with the number of transmit antennas, indicated by $M_\mathrm{t} \cdot P$. Under the fixed power constraint P, our analysis shows that a fully distributed configuration is optimal for the TOF-based localization scheme. In contrast, the AOA-based method benefits from concentrating antennas to enhance angle estimation accuracy, with an optimal deployment of eight BSs per square kilometre. When the power scales with the number of antennas $M_\mathrm{t} \cdot P$, the TOF-based approach favors a mixed configuration that blends centralized and distributed allocations, thereby balancing the beamforming gains with macro-diversity benefits.

Fig. 4 illustrates that an increase in the attenuation coefficient α makes a distributed allocation more advantageous. This occurs because distributing the antennas minimizes the average distance between service BSs and users, effectively diminishing interference from distant sources as both useful and interfering signals weaken over longer distances. On the other hand, when α is lower, centralized allocation becomes preferable since interference from remote BSs has a larger impact; despite the increased distance between BSs and users, the lower attenuation allows sufficient signal strength to be maintained. In Fig. 4, an optimal antenna ratio per BS of 1 indicates a massive MIMO configuration. Conversely, when this ratio approaches 0, the system effectively functions as a cell-free network. Moreover, as the cooperative area radius D expands (for instance, from 100 m to 200 m), the optimal fraction of antennas deployed at each BS relative to the total in the area decreases, reflecting the need for a denser antenna distribution near users to sustain high communication rates in larger cooperation zones.

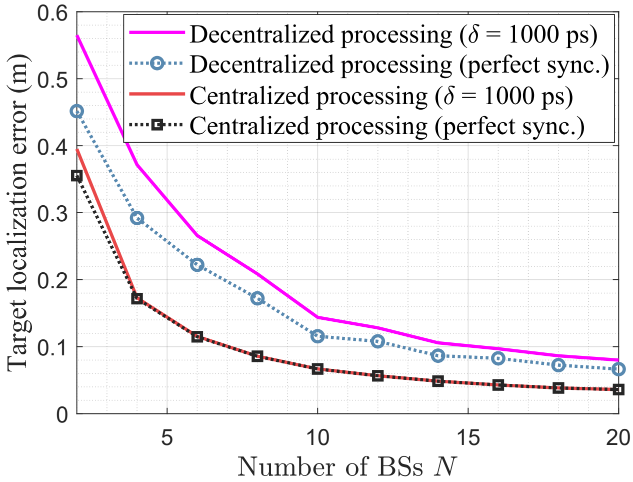

Fig. 6. Localization error comparisons between perfect time synchronization and time synchronization error (BS number increases with fixed area size).

Fig. 5 presents the performance boundaries defined in (31) for optimal joint and power allocation across two localization schemes, with a cooperation radius $D = 1000$ m. Notably, both TOF-based and AOA-based localization methods, significantly extend the performance frontier. Furthermore, overall sensing and communication performance improves with an increasing transmit antenna density, due to enhanced flexibility in resource allocation that boosts beamforming gains. As the bandwidth decreases, the performance of AOA-based localization becomes superior to that of TOF-based methods, primarily because the accuracy of TOF measurements deteriorates with reduced bandwidth.

In Fig. 6, $B = 10$ MHz, and the sync error is 1000 ps deviation. It can be found that in centralized processing, synchronization errors hardly affect the performance. This is mainly because the errors in the bidirectional bi-static links are of opposite signs and tend to compensate each other. Furthermore, with a sufficient number of localization BSs, the system achieves robust positioning. In contrast, decentralized processing relies solely on locally received signals, which prevents it from leveraging the compensatory benefits of the bidirectional bi-static link diversity. Consequently, performance under perfect synchronization is significantly superior to that observed with synchronization errors.

VII. Conclusions

This study introduces a novel cooperative ISAC network that integrates multi-static sensing with CoMP data transmission, utilizing cutting-edge localization techniques based on both AOA and TOF measurements. Our analysis reveals that strategically optimizing antenna-to-BS allocation, with a careful mix of centralized and distributed setups, substantially boosts performance by enhancing spatial diversity and coherent processing gains. In addition, we delve into the scaling properties of various localization methods and develop a comprehensive framework to assess communication data rates under different allocation strategies. This work not only advances our understanding of ISAC network dynamics but also lays the groundwork for future designs that address the dual challenges of sensing and data transmission in complex wireless environments.

References

[1] J. A. Zhang, F. Liu, C. Masouros, R. W. Heath, Z. Feng, L. Zheng, and A. Petropulu, "An overview of signal processing techniques for joint communication and radar sensing," *IEEE J. Sel. Top. Signal Process.*, vol. 15, no. 6, pp. 1295–1315, 2021.

[2] A. Liu, Z. Huang, M. Li, Y. Wan, W. Li, T. X. Han, C. Liu, R. Du, D. K. P. Tan, J. Lu, Y. Shen, F. Colone, and K. Chetty, "A survey on fundamental limits of integrated sensing and communication," *IEEE Commun. Surveys Tuts.*, vol. 24, no. 2, pp. 994–1034, Nov. 2022.

[3] K. Meng, Q. Wu, W. Chen, and D. Li, "Sensing-assisted communication in vehicular networks with intelligent surface," *IEEE Trans. Veh. Technol.*, vol. 73, no. 1, pp. 876–893, 2024.

[4] Y. Cui, F. Liu, X. Jing, and J. Mu, "Integrating sensing and communications for ubiquitous IoT: Applications, trends, and challenges," *IEEE Net.*, vol. 35, no. 5, pp. 158–167, Sep./Oct. 2021.

[5] K. Meng *et al.*, "Cooperative ISAC networks: Opportunities and challenges," *IEEE Wireless Communications*, pp. 1–8, 2024.

[6] K. Han, K. Meng, and C. Masouros, "Signaling design for noncoherent distributed integrated sensing and communication systems," *arXiv preprint arXiv:2501.18264*, 2025.

[7] R. Li, Z. Xiao, and Y. Zeng, "Toward seamless sensing coverage for cellular multi-static integrated sensing and communication," *IEEE Trans. Wireless Commun.*, vol. 23, no. 6, pp. 5363–5376, 2024.

[8] W. Shin, M. Vaezi, B. Lee, D. J. Love, J. Lee, and H. V. Poor, "Coordinated beamforming for multi-cell MIMO-NOMA," *IEEE Commun. Lett.*, vol. 21, no. 1, pp. 84–87, Jan. 2017.

[9] F. De Saint Moulin, C. Wiame, C. Oestges, and L. Vandendorpe, "Cooperative sensing in automotive urban scenarios using poisson line processes," in *2023 31st EUSIPCO*, 2023, pp. 720–724.

[10] K. Hosseini, W. Yu, and R. S. Adve, "A stochastic analysis of network MIMO systems," *IEEE Trans. Signal Process.*, vol. 64, no. 16, pp. 4113–4126, Aug. 2016.

[11] K. Meng, C. Masouros, A. P. Petropulu, and L. Hanzo, "Cooperative ISAC networks: Performance analysis, scaling laws and optimization," *IEEE Trans. Wireless Commun.*, vol. 24, no. 2, pp. 877–892, 2025.

[12] A. Salem *et al.*, "Rethinking dense cells for integrated sensing and communications: A stochastic geometric view," *IEEE Open J. Commun. Society*, vol. 5, pp. 2226–2239, 2024.

[13] T. S. Rappaport, Y. Xing, G. R. MacCartney, A. F. Molisch, E. Mellios, and J. Zhang, "Overview of millimeter wave communications for fifth-generation (5G) wireless networks-with a focus on propagation models," *IEEE Trans. Antennas Propag.*, vol. 65, no. 12, pp. 6213–6230, 2017.

[14] H. Q. Ngo, A. Ashikhmin, H. Yang, E. G. Larsson, and T. L. Marzetta, "Cell-free massive MIMO versus small cells," *IEEE Trans. Wireless Commun.*, vol. 16, no. 3, pp. 1834–1850, 2017.

[15] W. Cai, P. Wang, Y. Li, Y. Zhang, and B. Vucetic, "Deployment optimization of uniform linear antenna arrays for a two-path millimeter wave communication system," *IEEE Commun. Lett.*, vol. 19, no. 4, pp. 669–672, 2015.

[16] J. Li and P. Stoica, *MIMO radar signal processing*. John Wiley & Sons, 2008.

[17] P. Stoica and A. Nehorai, "MUSIC, maximum likelihood, and Cramer-rao bound," *IEEE Trans. Acoust., Speech, Signal Processing*, vol. 37, no. 5, pp. 720–741, 1989.

[18] J. Li and R. Compton, "Maximum likelihood angle estimation for signals with known waveforms," *IEEE Trans. Signal Process.*, vol. 41, no. 9, pp. 2850–2862, 1993.

[19] M. A. Richards *et al.*, *Fundamentals of radar signal processing*. Mcgraw-hill New York, 2005, vol. 1.

[20] M. Sadeghi, F. Behnia, R. Amiri, and A. Farina, "Target localization geometry gain in distributed MIMO radar," *IEEE Trans. Signal Process.*, vol. 69, pp. 1642–1652, 2021.

[21] K. Han, K. Meng, and C. Masouros, "Over-the-air time-frequency synchronization in distributed isac systems," *arXiv preprint arXiv:2503.08920*, 2025.

[22] J. Park, N. Lee, J. G. Andrews, and R. W. Heath, "On the optimal feedback rate in interference-limited multi-antenna cellular systems," *IEEE Trans. Wireless Commun.*, vol. 15, no. 8, pp. 5748–5762, Aug. 2016.